

MSC-33619

SIMULATION OF STRUCTURAL DYNAMICS
OF SPACE VEHICLES DURING LAUNCH

by

H. L. Runyan

NASA Langley Research Center

The purpose of this presentation is to concentrate on simulation techniques which are of importance in the design and operation of launch vehicles. We shall concentrate on dynamic problems from the time of lift-off to the time at which the vehicles leaves the sensible atmosphere. This time interval is relatively short, being of the order of just several minutes and to paraphrase an old adage "the first hundred seconds are the hardest."

To give some idea of the stable of NASA launch vehicles, the first figure illustrates most of the launch vehicles now in use or soon to be operational. The payload capabilities for a 300 nautical mile orbit range from about 300 pounds for the Scout vehicle to 200,000 pounds for the Saturn V. The Scout is the smallest vehicle and is the only solid propellant vehicle which has injected payloads into orbit. It is interesting to note that the Scout and the three Saturn configurations are the only vehicles developed solely as space research vehicles, the first stages of the remaining vehicles were developed strictly as military vehicles by the Air Force and have been adapted for space use. The Saturn V, now in the design and manufacturing stage, is 360 feet high, has a first and second stage diameter of 33 feet, has a lift-off

weight of 6,000,000 pounds and has a total thrust of 7,500,000 pounds. Except for the Scout, all vehicles are liquid propelled, are very thin skinned, and present many interesting and sometimes baffling dynamic problems during their ascent through the rather hostile atmosphere. Thus, to solve many of these dynamic problems, dynamic modeling techniques are not only convenient, but in some cases, mandatory.

What are some of the problems which are of concern to the dynamicist in designing and operating a launch vehicle? A listing of these problem areas is given in figure 2. On the top of the figure is shown "input" loading, which is imposed on a "system" - the launch vehicle, and the "output" load, in terms of stresses and acceleration.

Buffet and acoustic loads are closely related as can be seen by the general similarity of the outputs. Winds, both ground and aloft, can induce bending moments which can involve such severe loads that certain portions of the vehicle must be designed to accommodate these loads.

Fuel slosh in general is a control problem, however, loads can be induced into the vehicle if the liquid oscillations are not kept to a minimum. Control loads during programmed maneuvers are sometimes severe and, in particular, we must insure that excessive loads during maneuvers are not applied during periods of high loading from other sources. Recently, we have become concerned about response and loads in the longitudinal direction. Since 90 percent of the weight of a typical liquid propellant vehicle may be liquid, the coupling of the liquid system with the structure and engine is possible. During

lift-off, when the hold-down clamps are released, a large dynamic response takes place and is the principal design consideration for the bottom of the tanks. Another phenomena which has recently occurred on two vehicles is the coupling of the engine, turbopump, structure, and fluid components into a system that can become unstable. This has been referred to as the POGO problem, since the vehicle responds in a longitudinal direction, in the manner of a boy who is bouncing on a pogo stick.

In addition to creation of loads due to all of these sources of excitation, pilot performance is an additional quantity of great significance. During his ride through the many faceted environment, this required performance capability is due to the necessity of retaining his ability to read small indicators, to judge whether his flight is satisfactory, and perhaps to operate his abort system in case of a malfunction. Of course, this leads into an entirely new field which we will not touch on, namely the dynamic response and resonances of the human body to various frequencies and acceleration levels.

One of the unfortunate aspects of this loading picture is the simultaneity of the occurrence of these loads. In figure 3, a plot for various loading sources against time of flights is shown, where the black area indicates the probable time at which the particular event will occur. The point here is that it appears rather black between the transonic region and the maximum dynamic pressure region for most of the loading conditions. We are still at the point of

tyring to understand each problem separately. These combined loads present a rather complex interaction problem, which, at the present time, is not entirely understood. Some of the interaction effects that one could visualize, for instance, involve the influence of the vehicle bending, either statically due to winds or dynamically during the bending response due to gusts, on the local vibrating characteristics of the thin plates and shells and the response of these shell structures to such random forces as buffet and acoustics pressures.

Now let us look at the loading picture in more detail in figure 4, in terms of a preliminary design. On the right is a sketch of a tank containing a fluid of height h , density ρ , in an acceleration field a , with an internal pressure p above the fluid surface. The sketch at the left depicts an elemental section of the tank wall skin and indicates the loading.

The hoop stress then is given for a particular time of flight by

$$\sigma_H(x) = \frac{\text{Internal Pressure } pr}{t} + \frac{\text{Hydrostatic Pressure } h(x)\rho ar}{t}$$

From this elementary formula, one can make a preliminary selection of the material and skin thickness required. The longitudinal stress is then given by

$$\sigma_L(x) = \frac{\text{Internal Pressure } pr}{2t} + \frac{\text{Bending Moment } M_c}{I} - \frac{\text{Acceleration Drag } m(x)a + D(x)}{2\pi rt}$$

where M is the applied external bending moment due to wind, control gusts, buffeting, etc., $m(x)$ is the mass above the longitudinal station x , $D(x)$ is the total drag down to station x . From preliminary trajectory studies, the acceleration a is known as well as the drag $D(x)$. Of course, σ_L will vary around the circumference from a tension load to a compressive load when the vehicle bends. For the most part, the critical loading occurs on the compression side and since 2000 papers have been written over the years on the subject of shell buckling, this area will not be touched on. However, for thin unstiffened shells, a conservative approach would be to set $\sigma_L(x) = 0$. With a value of σ_L decided upon, we can then calculate the bending moment M , which is the vehicle structural capability remaining for such loads as winds, gusts, control, etc. A typical bending moment capability curve plotted against vehicle station is shown in figure 5. Notches in the capability curve are due to joints, and unpressurized areas such as interstage structure.

Now we finally come down to the reason for presenting this rather detailed discussion of the preliminary design of a launch vehicle, namely the estimation of the loads from remaining loading sources. The summation of these estimated loads is shown in figure 6 for a particular time of flight. Estimation of most of these loads requires a knowledge of the vibrational characteristics of the structures, involving not only the complete vehicle response (lateral as well as longitudinal motion), but local or isolated vibration of shells, trusses, mounting brackets, etc. As a typical example, we plot the load due to (1) control, for instance a preprogrammed pitch-over of the launch vehicle,

(2) wind loads caused by wind velocities as high as 250 mph, (3) gusts, (4) low frequency buffeting, due mainly to bulbous payload shrouds, (5) fuel slosh. The summation of these loads may approach the vehicle capability curve, thus an accurate estimation of these sources is necessary and dynamic models are playing a very important role in estimating these loads. To illustrate the role of various simulation techniques, figure 7 has been prepared to give our estimation of the state (of-the-art) of the various simulation techniques for studying the various problem areas. The darker the box, the higher the state-of-the-art and usage. Also included is an estimation of the relative cost of the various approaches, mathematical analysis being the least expensive and full-scale being the most expensive. In general, you can see that modeling for all phases is rather dark, and is highly competitive with mathematical analysis or full-scale testing.

DYNAMIC MODELING

The remainder of the paper will be concerned with specific examples of dynamic model testing. First, the problem of the gross vehicle vibratory motion will be considered, followed by a section on buffeting, and finally a few comments on the acoustic problem.

Lateral Bending Vibration Models

For lateral bending vibration, the governing differential equation is the well known beam equation

$$\frac{d^2}{dx^2} EI \frac{dy^2}{dx^2} = m\omega^2 y$$

where y is the lateral deflection, x is the length coordinate, E is the modulus of elasticity, and I is the section moment of inertia. The scaling parameter may then be defined as

$$\frac{m\omega^2 L^4}{EI}$$

Note that the geometric shape is not involved, thus we could obtain proper simulation by simply duplicating EI by a bar with ballast weights added to provide mass simulation. Of four models which we shall discuss for the lateral bending studies, only one followed this simplified path, the other three models utilized the same geometric shape, same material, the same ratio of tank radius to skin thickness.

One-Fifth-Scale Vibration Model of Saturn

Description. The 1/5-scale Saturn model described in reference 1, was built for the study of lateral bending vibrations; therefore, the important parameters to be scaled were the mass-stiffness ratios. Such things as aerodynamic fairing and fuel piping were not scaled since they

did not contribute to stiffness; however, lead ballast weights were used to simulate their mass. Furthermore, the vibrations of principal interest were the overall vehicle modes, so local panel stiffnesses were not scaled. Such things as fuel sloshing and the suspension system were considered to have a secondary effect on the overall vehicle vibration and so were not scaled for the initial part of the test. The model is shown on the left of figure 8, and the full scale vehicle is shown on the right in a vibration test tower.

The type of scaling chosen for the Saturn model was a component-by-component uniform reduction of dimensions to one-fifth of the full-scale values, using the same materials as the full scale. This replica type of scaling was chosen because of the structural complexity of the Saturn booster with the resulting difficulty of determining accurate equivalent stiffness and mass properties for the multiple-beam truss-work assemblies incorporated in the vehicle. An example of model duplication of a full-scale multiple-beam structure is shown in figure 9. This figure is a close-up view of the base of the vehicle and shows that structural details such as skin corrugations, built-up riveted beams, tension rods, and longitudinal stiffeners in the outer tanks have been duplicated on the model; however, details such as the number of rivets, aerodynamic fairing supports, and piping supports are not true scale reproductions.

Two important structural simplifications were made on the model. First the engines were simplified as shown in figure 10. Only the total weight, center of gravity, and moment of inertia were scaled.

The simulated engines were firmly attached at the gimbal point without attempting to scale actuator stiffnesses. Second, some ring frames were omitted from the shell structure of the second stage. A view of the aft end of the second stage showing its internal construction is shown in figure 11. About 70 percent of the second-stage weight is contained in the ballast tank at the center, which is supported by the eight radial trusses attached to the outer shell. The outer shell is attached to the first stage only at the eight points at the ends of the radial trusses and thus forms the principal load structure of the second stage. Several ring frames on the full-scale vehicle were omitted from the outer-shell load carrying structure on the model, resulting in some distorted vibration results which will be discussed subsequently.

Scaling. The Saturn model was scaled by selecting a length scale factor L_m/L_p of 1/5 and using the same materials on the model as on the prototype. Therefore, the following relations are established:

$$\frac{E_m}{E_p} = \frac{\rho_m}{\rho_p} = 1$$

Then, in order to maintain the dimensionless ratios for lateral vibrations, the mass and time scale factors must be:

$$\frac{M_m}{M_p} = \frac{1}{(5)^3}$$

$$\frac{\tau_m}{\tau_p} = \frac{1}{5}$$

Other relationships between model and prototype parameters, resulting from the dimensionless ratios, are:

1. Mass moment of inertia: $\frac{I'_m}{I'_p} = \frac{1}{(5)^3}$

2. Bending stiffness: $\frac{(EI)_m}{(EI)_p} = \frac{1}{(5)^4}$

3. Bending frequency: $\frac{f_m}{f_p} = 5$

4. Slosing frequency: $\frac{f_m}{f_p} = \sqrt{5}$

5. Shell frequency: $\frac{f_m}{f_p} = 5$

Comparison of the bending and sloshing frequency ratios shows that the full-scale bending-sloshing frequency relationship is not maintained on the model. Thus, the interaction of vehicle bending with sloshing on the model will not represent directly the full-scale situation. For the Saturn configuration, where the first sloshing frequency is lower than the first bending frequency, the reduction to model size separates the frequencies, thus tending to uncouple the sloshing from the bending modes. The shell frequency relationship is based on an unstiffened shell with the same material and internal pressure in both model and full scale. Comparison of the bending with the shell frequency ratio shows that interaction of

local shell vibration with vehicle bending vibration should be the same on the model as on the full scale in those cases where model construction and internal pressure are the same as the full scale.

Results. Some results of the model vibration test are shown in figures 12, 13, 14, and 15. In figure 12, the first vibration mode of the model and full-scale vehicles is shown with the vehicle ballasted to simulate the maximum dynamic-pressure weight condition. This figure shows almost exact agreement between model resonant frequency, when adjusted by the scale factor, and the full-scale resonant frequency. In order to obtain such good agreement, it was necessary to duplicate, on the model, the suspension system used to simulate free-free boundary conditions on the full-scale vehicle. The mode shapes of the full-scale and the model are in good agreement as can be seen from comparison of the circles with the square symbols. The booster outer tanks, which are free to deflect independently of the center tank except at their ends are shown in this figure to have the same deflection as the center tank, and this mode has the appearance of the more conventional bending modes obtained from non-clustered vehicles.

In contrast, the second vibration mode, shown in figure 13, shows one of the unusual vibration modes associated with the clustered arrangement of the Saturn booster. There is about a 10-percent difference in frequency between model and full scale in this mode, and comparison of the circles with the squares shows fairly good agreement of model with full-scale mode shape. The typical outer tank indicated by the flagged symbols is seen to deflect in the opposite direction as the center tank. Cross-section A-A at the

midsection of the booster shows that when the center tank deflects upward as indicated by the arrow, the outer tanks are deflecting independently in the downward direction. This unusual mode shape where the outer tanks deflect in the opposite direction from the center tank is associated with the clustered arrangement of the booster tanks and has been termed a cluster mode.

The effect of omission of the ring stiffeners from the outer shell of the second stage is illustrated by figure 14, which shows the fourth vibration mode of the 1/5-scale Saturn model. In the area of the second stage, two deflection curves are shown. The open circles indicate the deflection of the outer shell and the solid circles the deflection of the inner ballast tank. The data indicate that the outer shell and the ballast tank are deflecting in the opposite directions. This can be explained by examination of cross-section B-B. The solid lines in this sketch indicate the undisturbed position of the water-filled ballast tank, the eight radial trusses, and the outer shell; the data points indicate the experimentally determined vibration amplitude. This cross section shows that the outer shell is vibrating in a shell mode with seven waves, while the center tank is translating. The deflection measured at points A and B on the inner and outer tanks, respectively, are in opposite directions, as shown also in the sketch in the center. The shell mode in the second-stage outer shell shown here was observed on the model in the higher-frequency modes for most weight conditions; however, no shell modes in the second stage were observed on the full-scale Saturn vibration test vehicle.

The mode shapes and resonant frequencies which have been shown were measured at the weight condition which simulates flight near maximum dynamic pressure. An indication of how the resonant frequencies of model and full scale compare at other weight conditions is shown in figure 15. The ordinate is full-scale frequency, in cycles per second, and the abscissa is water level in the booster stage, in percent. Zero percent corresponds to first-stage burnout while 100 percent corresponds to lift-off. The previously shown data were measured at 48 percent full. Model frequencies, adjusted by the scale factor, are shown as circles while full-scale frequencies are shown as squares. The first bending mode frequency shows almost exact agreement except at lift-off, where the model frequency is about 7 percent high. The first cluster mode frequency is predicted by the model to within 10 percent. For higher modes, agreement between model and full scale is not as good.

The data presented in figure 15 were obtained using an eight-cable suspension system which duplicated a similar suspension system used for full-scale tests. Earlier model tests, using a two-cable free-free suspension system which gave much better separation between suspension frequency and bending frequency than the eight-cable system had given model first bending frequencies 5 to 10 percent lower than full-scale frequencies. This result indicated the importance of properly accounting for suspension system effects in comparing model and full-scale data and of properly interpreting ground test data when extrapolating to flight conditions.

Saturn V Dynamic Models

Figure 16 illustrates the present modeling project, which is a 1/10 scale replica model of the Saturn V. The model is 36 feet high, including the Apollo payload. The general type of construction of the full scale is shown including skin stringer, waffle pattern, integrally milled stringer, and corrugated skin. The model will duplicate all of these essential details up to the Apollo payload.

On the right of figure 16 is shown a scalloped or multicelled tank concept, which is also being constructed and will replace the cylindrical first stage for later tests. This concept has the advantage of higher fuel slosh frequencies, thus separating the control or pitch frequency from the fuel slosh frequency.

As an example of the construction detail adhered to in the model, figure 17 illustrates the interior of the first stage fuel tankage. Note in particular the detail in the fuel slosh baffles which are the thin, corrugated rings located on the circumference of the tank. The three corrugated pipes are three of the five tunnels which carry the fuel through the bottom tank to the five individual pumps for each engine. For the Apollo payload, beam simulation techniques are being used, whereby the structural and mass distributions are matched with no attempt being made to simulate the actual tankage construction.

In addition to the 1/10-scale model, a 1/40-scale model is being constructed which is shown in figure 18. An illustration of the details of the model construction is shown in figure 19. The modeling

concept for this case involved only the duplication of the mass and stiffnesses and does not follow the replica concept. On the lower left is shown the five-engine simulation. Next to the engine are two fuel slosh simulators, using a "bird-cage" spring-mass assembly. These simulators can be placed at various positions on the vehicle, and the spring constants as well as the mass can be changed in order to study the effect of fuel depletion. Thus, we will be able to study the coupling of fuel slosh with the elastic modes by spring constant and mass changes, in ranges of parameters not possible with liquids in a one "g" field.

Titan III

In addition to the NASA vehicle described, the Air Force has decided on scale model testing of the Titan III launch vehicle as shown in figure 20. This vehicle utilizes a modified Titan II as a center "core" on which two 100 inch diameter solid propellant boosters are strapped at two points. The length scaling factor selected here was 1/5, with the propellant tanks and interstage structure being rather faithfully reproduced by use of the same material as the prototype with the same ratio of tank radius to skin thickness.

This model was designed and constructed by the Martin-Marietta Co. of Denver, Colorado. It is not being tested in the Dynamics Research Laboratory at Langley Research Center by Martin Company personnel with the assistance of Langley engineers.

Fuel Slosh

One of the problem areas in testing liquid-fueled dynamic models is the effect of the coupling fuel slosh with other modes. In figure 21, several significant frequencies are plotted against flight time for the cylindrical tank as well as the scalloped tank for a vehicle in the Saturn V class. The first bending mode frequency variation is shown as a dashed line, flight fuel slosh frequency variation as a solid line, range of pitch frequency by the shaded area, a line depicting a 1/10-scale model fuel slosh frequency and a line illustrating fuel-scale ground test frequencies. A rather large separation in frequency exists between the first bending mode and the flight fuel slosh frequency. Thus, coupling of the fuel slosh mode with the elastic mode will be rather weak even in the flight case. A 1/10-scale model would have lower fuel slosh frequencies as indicated, but since the fuel slosh is already rather well uncoupled from the bending mode, the 1/10-scale model results should duplicate the full-scale flight results with very minor differences. As a matter of fact, even for full-scale ground tests, the proper fuel slosh frequency would not be exactly simulated as shown due to the 1 g field in which the vehicle must be tested.

On the right side of figure 21 is shown the effect of the system frequencies of a scalloped tank wherein only the first stage of the complete vehicle has been changed from the cylindrical tank to the scalloped tank. Note that the bending frequency has been reduced. This is due

to the basic design criteria of maintaining the same internal pressure and vertical load-carrying ability as in the cylindrical tank. This results in more material being used closer to the tank center thus reducing the moment of inertia and consequently the bending stiffness. On the other hand, the fuel slosh frequency has increased due to compartmentation. Thus, the two frequencies are approaching each other while moving the fuel slosh frequency away from the rigid body frequency, which, of course, is beneficial. However, a coupling between fuel slosh and the fundamental vibration modes now exists. In cases such as this, the adequacy of the structural duplication of the model may be checked against analytical representation for fuel slosh frequencies well removed from the coupling possibility. Then with confidence in the structural adequacy of the model, the effect of fuel slosh having frequencies in the neighborhood of the fundamental elastic frequencies may be estimated for control system design by calculating the effect by utilizing the spring-mass or pendulum fuel slosh analogies.

Buffeting

Now let us turn our attention to buffeting. The term "buffeting" is really not very well defined and precise. For the purposes of this paper, we shall consider the term "buffet" to refer to aerodynamic flows involving departure from potential flow with consequent flow breakdown and separation which can result in structural response of the vehicle. Obviously, this is a rather broad definition and is symptomatic of the wide spectra of buffet problems.

The occurrence of buffeting on launch vehicles has been a surprise to many people; the long cylindrical shape of typical launch vehicle did not appear at first to offer any substantial problem. However, certain vehicle failures in the early days of the space program were diagnosed to have been due to possible flow breakdown, inducing loads that could result in structural failure.

The following material and figures are taken from an excellent talk given by A. G. Rainey of Langley Research Center (reference 2) which was presented at the Fifth Annual AIAA Structures and Materials Conference in April, 1963 and covers the status of buffet research at that time.

Recognizing that there are many types of buffet, two general types of buffet are illustrated in figure 22. The power spectral density of the oscillating pressure is plotted against frequency. The ordinate indicates the relative "power" or pressure generated at a particular frequency. The integration of the area under the curve is the mean square of the pressure oscillation. The curve and figure on the left illustrate one type of buffeting that could be obtained on a nose or payload fairing shape in which the diameter is reduced in the direction of flow. Here the flow breaks down, alternately on the top and bottom of the fairing due to a rather shallow reverse angle on the rear part of the fairing during part of the transonic flight. As illustrated by the plot of the spectra, the predominant frequencies of the phenomena are rather low and, as a matter of fact, fall within the range of the fundamental bending vibration modes of the complete vehicle. A considerable

amount of research has been accomplished in this area, and there are some rough guides concerning the relationship of this reverse angle and the magnitude of the buffet pressures. Actually, if the angle were increased to 90° i.e. a step change from the larger diameter front section to the smaller diameter rear section, this low frequency buffet would be eliminated since the shock position and the turbulence would now be fixed at a given location and the possibility for it to oscillate from one side to the other is eliminated. However, this step could lead into another type of buffet which is of importance from the standpoint of local or small areas of the vehicle. An illustration of the type of buffet is shown rather dramatically in the sketch on the right of figure 22. Here we have buffeting due to attached shocks and boundary layer build up and collapse, due to flow through the open structure supporting the abort rocket motor and as well to a reverse angle due to the adapter. Note the spectra shape which contains nearly an equal amount of power throughout the frequency band from 0 to 220 cps, however, it is not as severe as for the bulbous nose shape, although the area under the curve, representing the mean square is about the same. Unfortunately, most of the panels and equipment as well as the astronaut can respond to some frequency in this range. Thus, consideration of this high frequency buffet must be taken into account in the design of the launch vehicle system.

Theoretical techniques for predicting these spectra do not exist, therefore, the dynamic model enters the picture. Dynamic models have been used to study both types of buffet. For the low frequency buffet,

the governing differential equation will be the usual beam equation, with the addition of a number of parameters which have been obtained mainly from our previous experience with aircraft buffet. The equation is

$$\frac{d^2}{dx^2} EI \frac{d^2 y}{dx^2} = m\omega^2 y + f \left[\frac{r}{L}, \frac{v}{a}, \frac{\rho v l}{\mu}, \frac{m}{\rho_f}, c/c_r, \frac{L\omega}{v} \right]$$

where r/L signifies geometric similitude, v/a is Mach number, $\rho v l / \mu$ is Reynolds number, m/ρ_f signifies the ratio of the mass of the model to the mass of the surrounding fluid, $L\omega/v$ is the familiar reduced frequency parameter and c/c_r is the structural damping ratio. All of these parameters can be faithfully reproduced in our present tunnels by the use of dynamic models, with the possible exception of Reynolds number and damping. However, we believe that as long as the full scale vehicle has Reynolds numbers in the turbulence boundary layer range and our models reproduce Reynolds numbers well into this same range, the effect of Reynolds numbers is of secondary importance. The structural damping usually turns out to be within the range found in the full scale vehicle.

With a scaled model-wind tunnel combination satisfying the above criteria, the measured quantities of interest will be buffet pressures and bending moment power spectral densities. The relation between model and full scale power spectral density pressure is

$$\frac{P(\omega)V}{q^2 L}$$

while for the bending moment, the power spectral density is

$$\frac{P(\omega)V}{q^2 L^7}$$

One of the unfortunate aspects of modeling technology is the lack of adequate full scale results for correlation, consequently, the proof of scaling laws is, in many instances, substantiated by utilizing models having different scale factors. An example of this aspect of modeling is shown in figure 23, for the Apollo-Saturn I space vehicle. The measured random pressure was obtained on the service module which is just below the Apollo spacecraft. The top curve represents the power spectra density of pressure divided by the square of the model dynamic pressure plotted against model frequency. Two models are shown, a 1.6 percent model and an eight percent model. Note the large differences between the curves. When the similarity parameter for the power spectral density is applied, the curves are brought rather closely together, thus indicating that we are not violating or neglecting large scaling parameters.

An example of the buffet model utilizing these scaling laws is shown in figure 24, which is an eight percent dynamic simulation for the Apollo-Saturn I space vehicle. The basic structural stiffness is duplicated by a hollow cylindrical tube of varying diameter to approximate the stiffness; mass was simulated by the addition of weights, and the whole structure covered by rings of styrofoam to provide the proper aerodynamic shape. These tests were very successful, results being utilized to predict the buffet bending moment for the full scale

vehicle. An example of the results is shown in figure 25, where the bending moment is plotted against vehicle station. The solid curve represent the RMS of the buffet bending moment, the dashed lines represent the contribution from each of the first three vibration modes. Of major significance is the very large contribution due to the second bending mode. Apparently the input was of such a nature as to have frequencies and phases as to cause a large response in this mode.

The previous discussion has been concerned with the low frequency buffet problem. We feel that, in general, the technology has advanced sufficiently so that rather reliable results may be obtained. The picture for higher frequency buffet, of importance for panel response, equipment environment, and astronaut performance, is rather foggy at the present time. The main reason for this difficulty is the introduction of the thin, elastic shell into the problem. Even the governing differential equations appear in many ramifications, depending on the approximations used to obtain the equations. When the vibration amplitude is greater than the skin thickness, nonlinear effects may take over; plate characteristics are sensitive to small changes in the boundary conditions (temperature differences as well can cause large changes in the panel response). In the face of these difficulties, efforts are underway to search for means for solving the problem. Based on examination of the governing differential equation, on previous buffet experience, the following list of parameters are thought to be the more significant:

- | | |
|-------|--|
| r/L | Geometric ratio (radius to length) |
| r/t | Ratio of tank radius to skin thickness |

r/h	Ratio of tank radius to fluid height (in cases of tanks containing a propellant)
$\frac{\rho_l}{\rho_a}$	Ratio of fluid density to air density
μ	Poissons ratio
P/E	Ratio of internal pressure to modulus of elasticity
$\frac{\rho \omega^2 L^2}{E}$	Ratio of dynamic to elastic forces
$L\omega/V$	Reduced frequency

The technique now being followed to perfect a technique for studying this high frequency buffet problem, is to resort to replica (or very detailed) dynamic modeling. In order to provide a model that can be used for basic research as well as provide information of immediate use in NASA's largest and most significant program, the service module of the Apollo-Saturn configuration was chosen as a sample case. The model is being constructed of the same material as the prototype, all rings and stringers are being duplicated, and even the rivet size and spacing is a very close approximation of the actual structure. Figure 26 shows a photograph of the parts of the 1/10 scale model now under construction. The three sections of the service module are shown before the installation of the skin. This reproduction has gone to the extent of attempting to scale the rivets, where were made by hand from a aluminum wire. Tests will be made on this model in the near future. This concludes the discussion of buffeting, but let us turn our attention now to a closely related topic, acoustics.

Acoustics

The subject of acoustics is in some instances closely related to buffet, in other cases the relationship is not clear. In the first instance, noise can be generated by flow breakdown and separation just as in the case for buffet, during transonic and low supersonic flights. In the other case, the noise source is the engine, important during lift-off phase and early flight and its effect is in the more classical since the source of the noise is some distance from the point of interest. For this case, we are not only interested in the noise effect on the vehicle itself, but also on the buildings, equipment, and personnel in the vicinity of the launch site. As a matter of fact, a large amount of property has been purchased by the NASA at Cape Kennedy in order to insure that sufficient distance between the new launch sites and populated areas will be maintained in order to reduce the community noise problem.

In testing for vehicle acoustic response, noise will usually be focused on relatively small areas, and thus testing of full scale components is becoming the accepted practice. Langley Research Center has gradually built up a number of specialized facilities ranging from anechoic chambers, heated noise jets, to a new ultra low frequency testing chamber. As a matter of fact, the first specimen to be tested in the new low frequency facility is full scale and involves the response of humans to high intensity noise in the range of 0 to 50 cps. This sub-audible and near sub-audible range is of extreme importance

since most of the power in the characteristic engine noise spectra of the new larger launch vehicle will be concentrated in this low frequency range. This new facility consists of a tank 24 feet in diameter and will handle a full scale Apollo spacecraft. Tests on the spacecraft will be made at a later time. This concept has already been used in the case of the Mercury spacecraft. The 9 x 6 foot thermal structures tunnel is a blow-down tunnel and intense noise fields are generated at its exit. This noise field has been rather extensively surveyed and it has been found that the intensity (db's) and spectra shape rather closely approximate that which has been measured during early unmanned flights of the Atlas. Thus, a full-scale capsule including a full-scale human was placed in the appropriate position near the exit of the 9 x 6 foot tunnel and exposed to the noise field. Problems of astronaut communication and equipment functioning were then studied.

Many specimens are under test in the various facilities, with a good deal of attention being paid to the fatigue problem. A general discussion of work in the acoustic field is given in reference 3. As an illustration of a current research study, we are studying the response of a typical launch vehicle tank to sinusoidal inputs due to both a point source of excitation as well as sinusoidal acoustic inputs. Ultimately, we hope to impose random noise on the tank, and, utilizing the information obtained from the sinusoidal tests, predict the random response of the tank. The tank being used in these tests is one of the cluster tanks from the first stage of the 1/5 scale model of Saturn I,

which has been previously discussed. The tank is 11 feet long, 14 inches in diameter.

The tank has been installed in the Langley Research Center Anechoic Chamber and figure 27 illustrates the test set-up. The tank may be oscillated by means of the shaker or by a siren having discrete input frequency, or by an air jet located near the model. In a theory of response of structures to noise, reference 4, it is shown that the response is proportional to the radiation resistance, i.e., its noise radiation properties when vibrated. Since the tests are being performed in an anechoic chamber, the sound radiation from the tank may be measured by means of surrounding microphones during tank mechanical vibrations.

In figure 28, the acceleration response of a point midway on the tank, due to a 1 pound slowly varying sinusoidal force applied by a shaker at one end of the tank, is shown. The figure illustrates the acceleration response for an empty tank and a tank full of water. The surprising result that the numerous responses for both cases were relatively the same, where the large response peak for the lowest frequency for the full case was simply shifted to a lower frequency.

Concluding Remarks

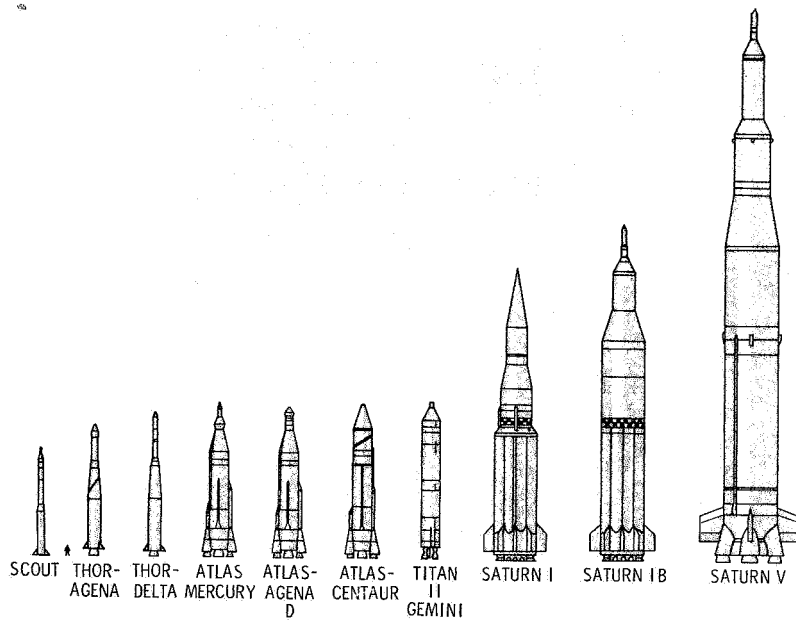
The use of reduced scale physical models and the areas requiring full scale tests for the solution of dynamic problems have been pointed out. In general, modeling technology for the solution of dynamic

problems of launch vehicles has been recently updated through a rather broad and vigorous research program, and a good foundation now exists for the solution of many of these perplexing problems.

The areas requiring additional work are usually associated with small sections of the vehicle and involve the difficult problem of estimation of response of a shell type structure to random buffet and/or acoustic sources. The combined loads problem involving the correlation of the various loading sources is still not settled and much research is required in this area.

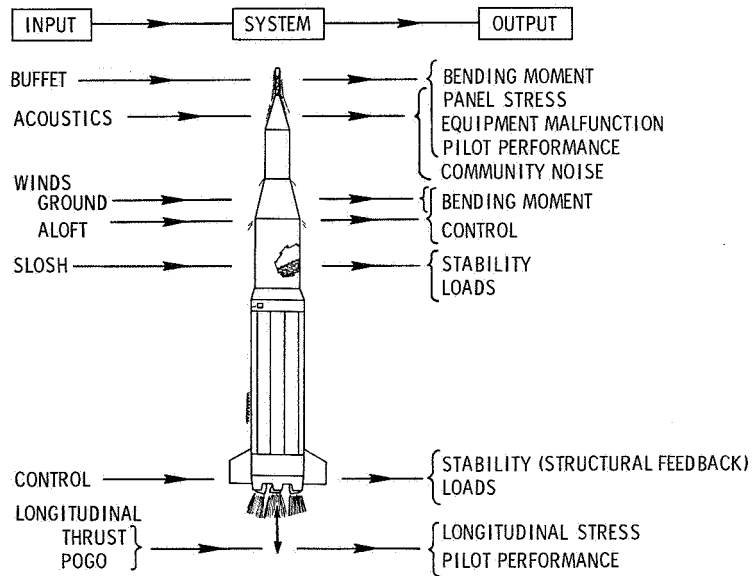
REFERENCES

1. Mixson, J. S., Catherine, J. J., and Arman, Ali: Investigation of the Lateral Vibration Characteristics of a 1/5-Scale Model of Saturn SA-1. NASA TN D-1593, 1963.
2. Rainey, A. Gerald: Progress on the Launch-Vehicle Buffeting Problem. Presented at the Fifth Annual AIAA Structures and Materials Conference, April 1-3, 1964, Palm Springs, California.
3. Edge, Phillip, M., Jr., and Rucker, Carl E.: Response-To-Noise Studies of Some Aircraft and Spacecraft Structures. Presented at the Second International Conference on Acoustical Fatigue, April 29 - May 1, 1964, Dayton, Ohio
4. Crandal, Stephen, ed. Random Vibration, Volume 2. MIT Press. Chapter 7.



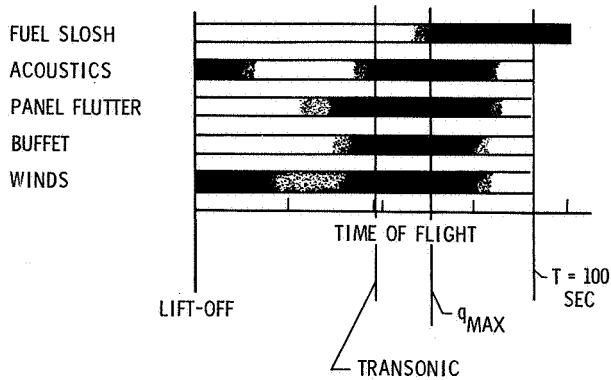
NASA

Figure 1.- NASA launch vehicles.



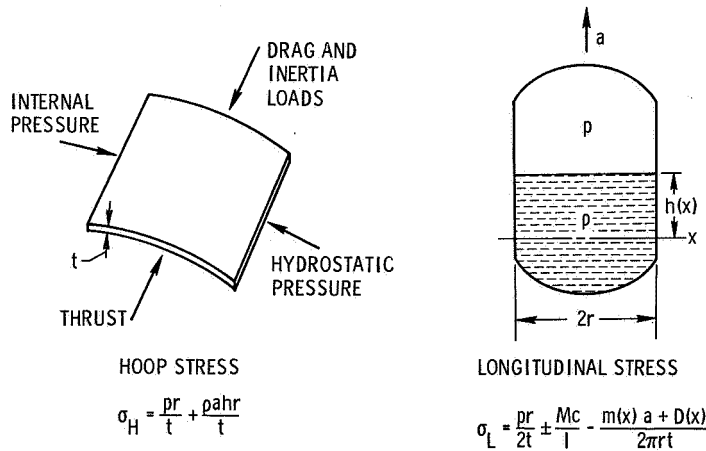
NASA

Figure 2.- Structural dynamic loading.



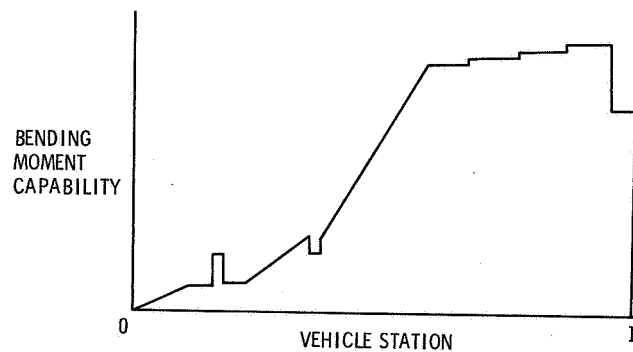
NASA

Figure 3.- Loading conditions versus time of flight.



NASA

Figure 4.- Preliminary design considerations.



NASA

Figure 5.- Bending-moment-capability curve for a launch vehicle.

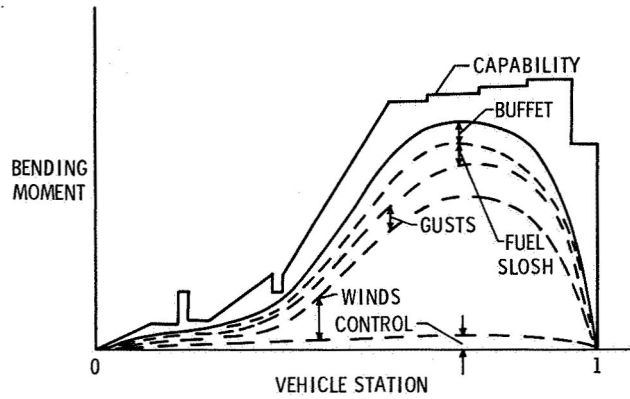


Figure 6.- Bending-moment capability and applied loads.

NASA

(MORE ADVANCE TECHNOLOGY HAS THE GREATER NUMBER OF LINES)

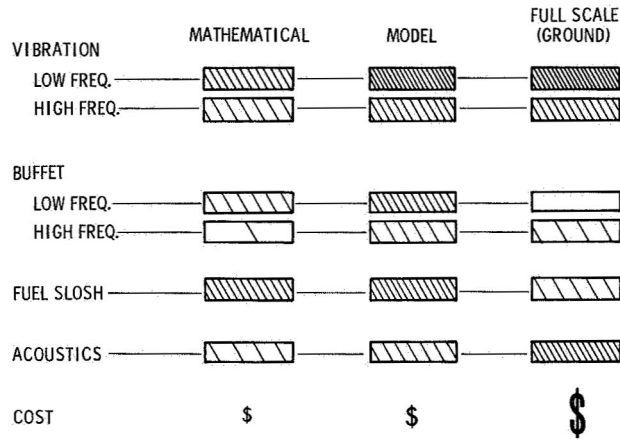


Figure 7.- Estimation of status of simulation techniques for launch vehicles.

NASA

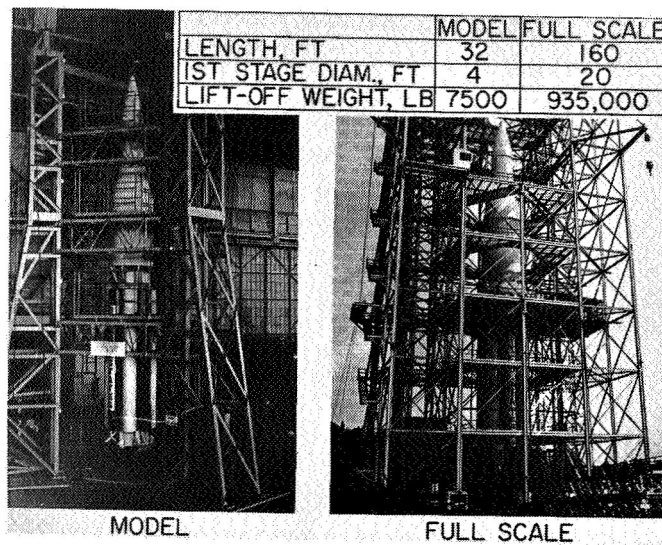
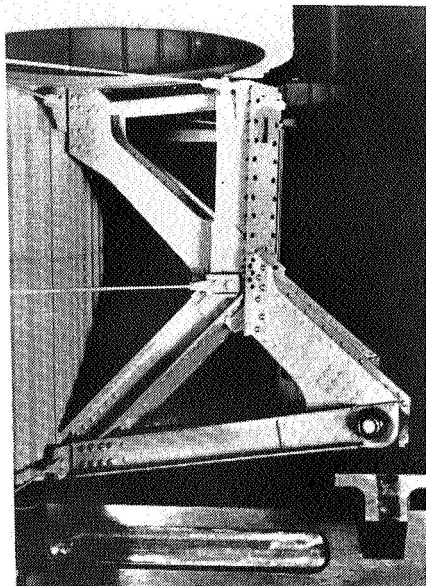
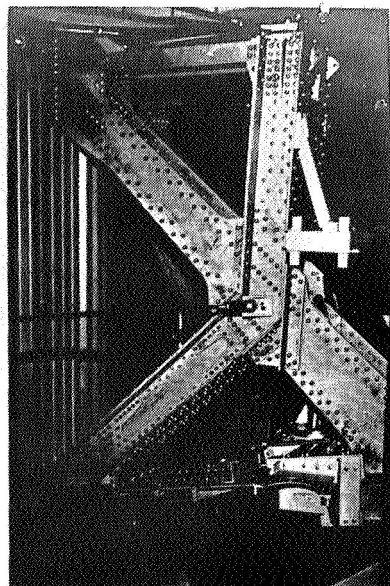


Figure 8.- Saturn vibration-test vehicles.

NASA



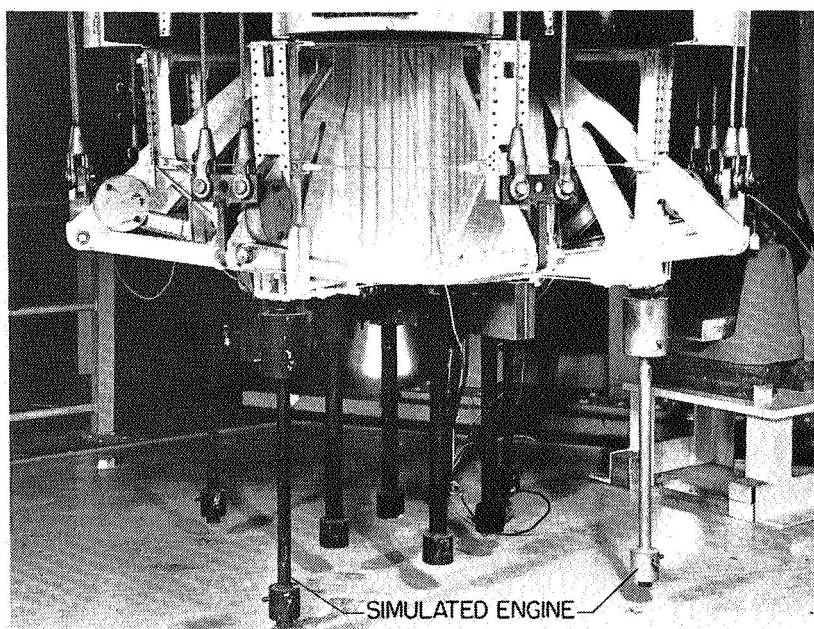
MODEL



FULL SCALE

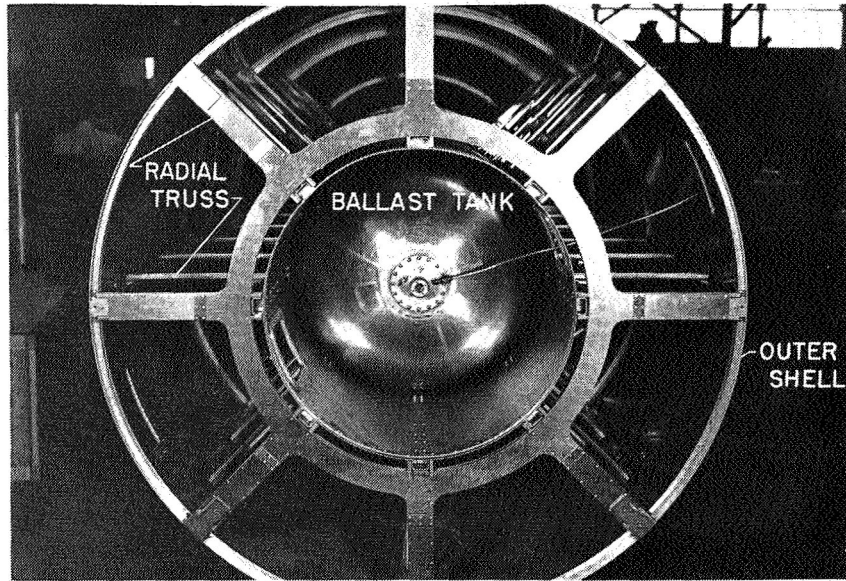
NASA

Figure 9.- Saturn structural details.



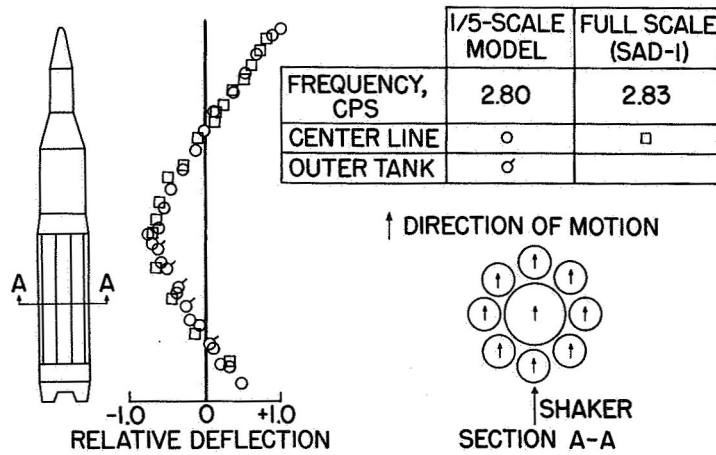
NASA

Figure 10.- Photograph showing 1/5-scale Saturn engines.



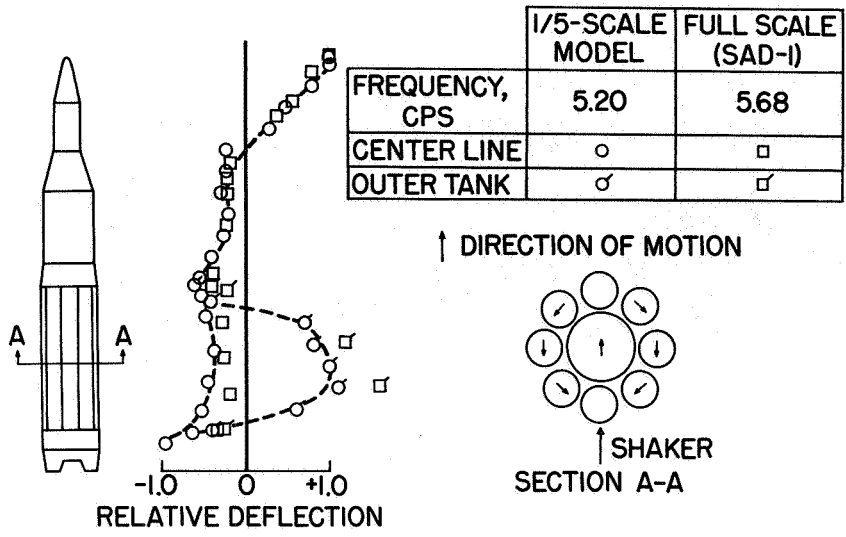
NASA

Figure 11.- End view of 1/5-scale Saturn second stage.



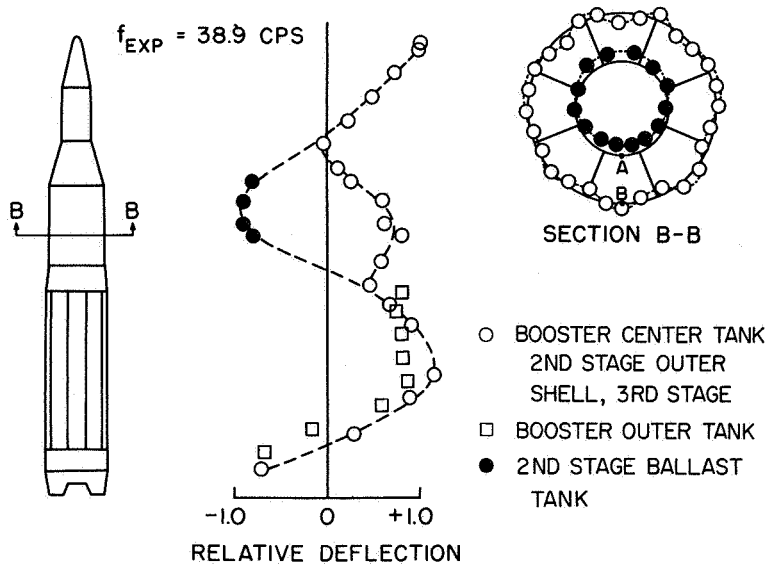
NASA

Figure 12.- First bending mode of Saturn, maximum dynamic pressure weight.



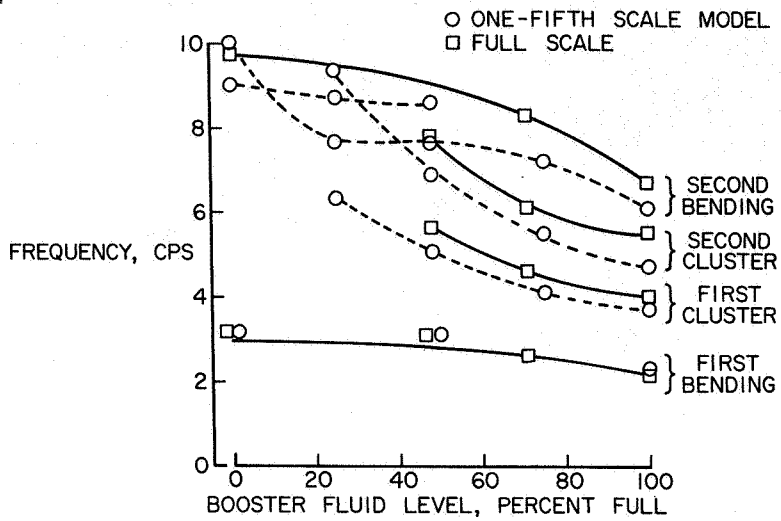
NASA

Figure 13.- First cluster mode of Saturn, maximum dynamic pressure weight.



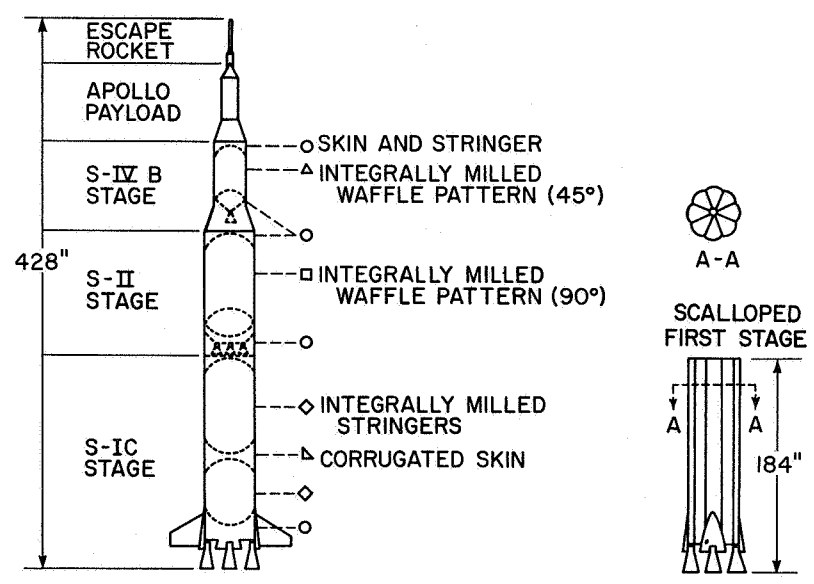
NASA

Figure 14.- Fourth vibration mode of 1/5-scale Saturn.



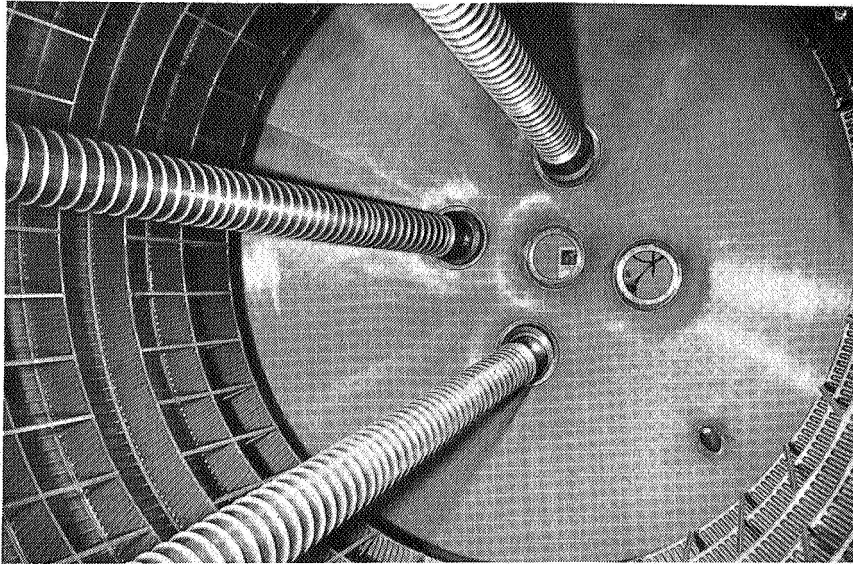
NASA

Figure 15.- Fundamental vibration frequencies of Saturn I.



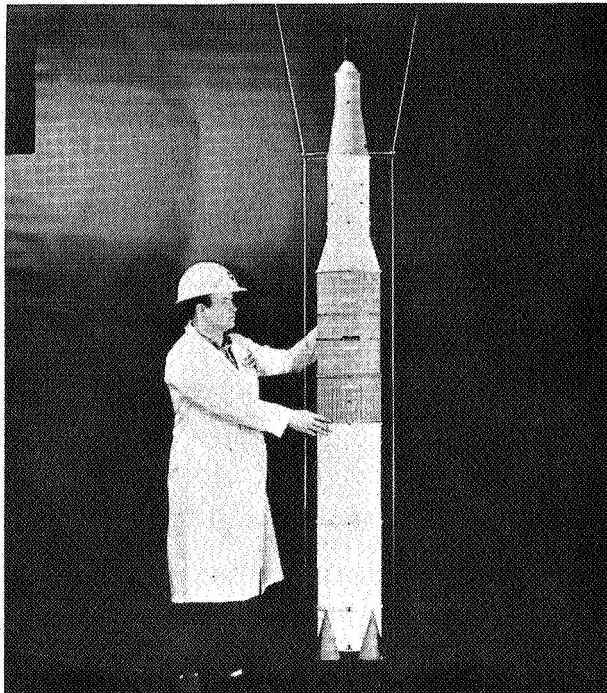
NASA

Figure 16.- 1/10-scale model of Saturn V and scalloped first stage.



NASA

Figure 17.- Internal view of Saturn V model fuel tank.



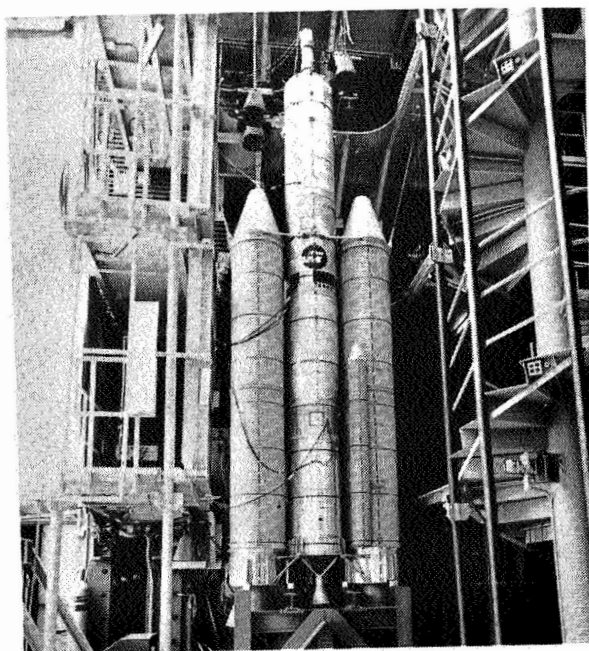
NASA

Figure 18.- 1/40-scale model of Saturn V.



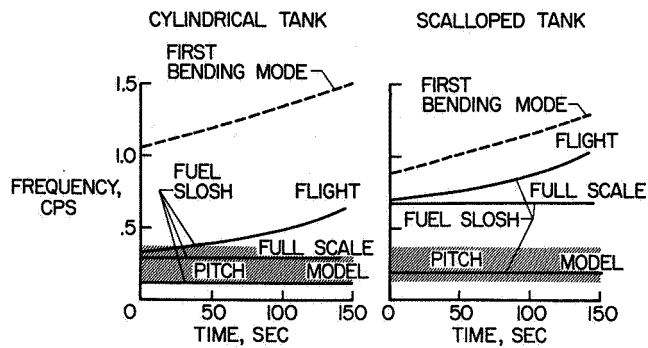
NASA

Figure 19.- 1/40-scale model details of Saturn V.



NASA

Figure 20.- 1/5-scale model of Titan III in dynamic test tower.



NASA

Figure 21.- Fundamental frequencies calculated for large launch vehicle for cylindrical and scalloped first stage.

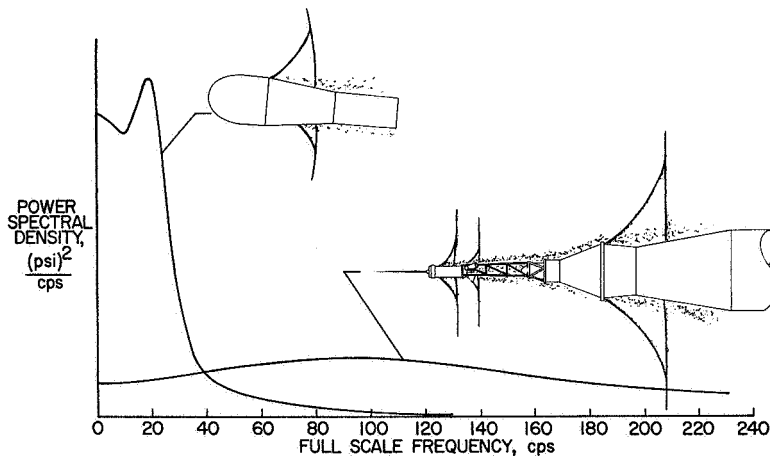


Figure 22.- Two types of buffet pressure spectra.

NASA

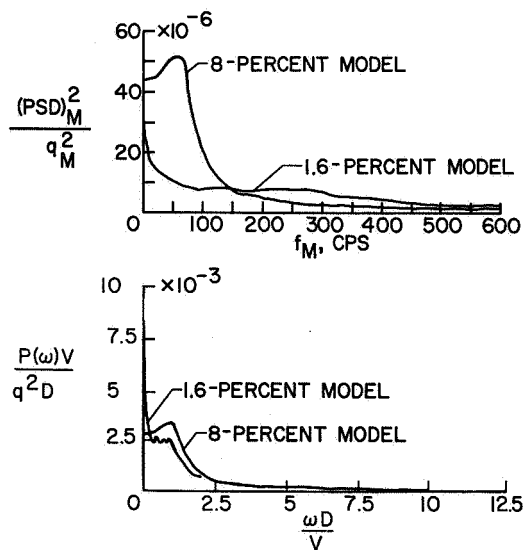
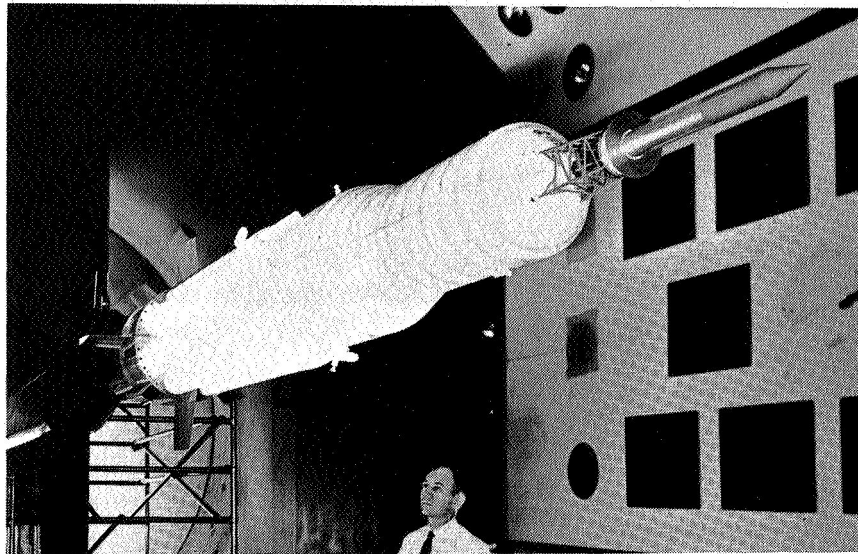


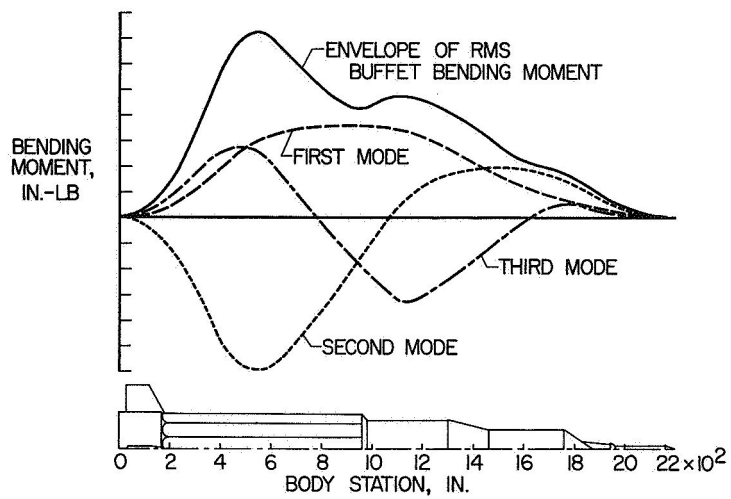
Figure 23.- Scaling of buffet pressure spectra.

NASA



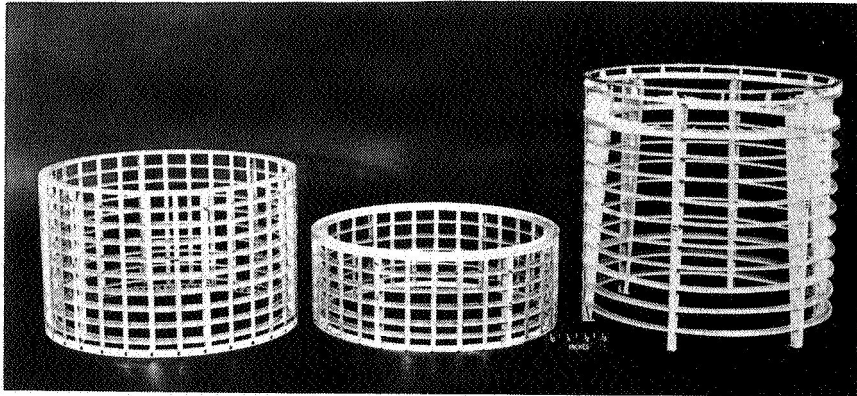
NASA

Figure 24.- 8-percent buffet model mounted in tunnel.



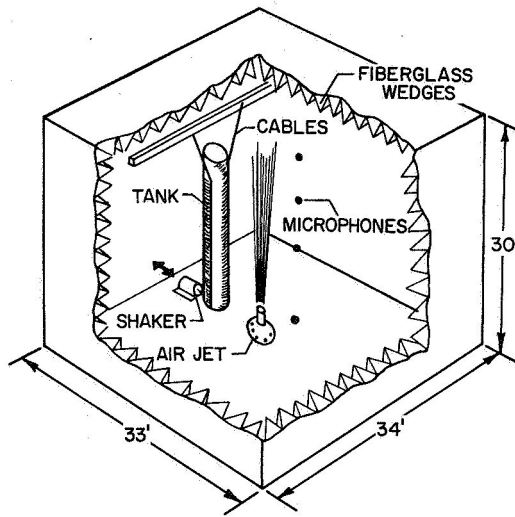
NASA

Figure 25.- Modal contribution to buffet bending moment predicted from Saturn-Apollo model results.



NASA

Figure 26.- Parts for 1/10-scale replica model of Apollo service module.



NASA

Figure 27.- Tank response.

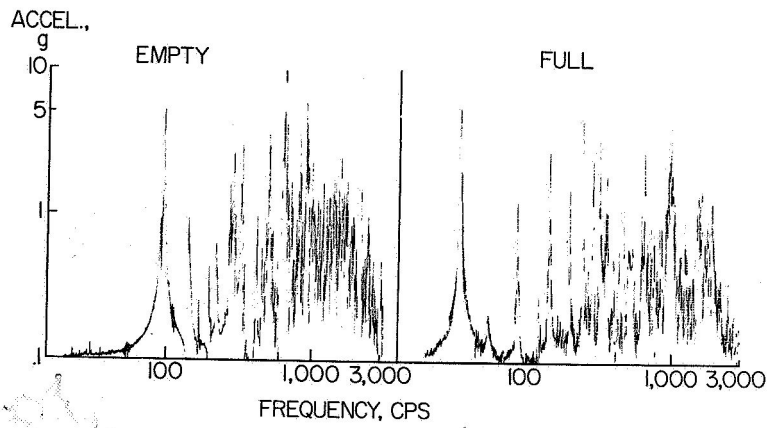


Figure 28.- Response of 1/5-scale Saturn with and without fuel.

NASA